

MeV neutrino dark matter: Relic density, lepton flavour violation and electron recoil

Juri Fiaschi,^a Michael Klasen,^a Miguel Vargas,^b Christian Weinheimer,^b and Sybrand Zeinstra^a

^a*Institut für Theoretische Physik, Westfälische Wilhelms-Universität Münster, Wilhelm-Klemm-Straße 9, 48149 Münster, Germany*

^b*Institut für Kernphysik, Westfälische Wilhelms-Universität Münster, Wilhelm-Klemm-Straße 9, 48149 Münster, Germany*

E-mail: fiaschi@uni-muenster.de, michael.klasen@uni-muenster.de,
weinheimer@uni-muenster.de, m_varg03@uni-muenster.de,
swzeinstra@uni-muenster.de

ABSTRACT: Right-handed neutrinos with MeV to GeV mass are very promising candidates for dark matter (DM). Not only can they solve the missing satellite puzzle, the cuspcore problem of inner DM density profiles, and the too-big-to fail problem, *i.e.* that the unobserved satellites are too big to not have visible stars, but they can also account for the Standard Model (SM) neutrino masses at one loop. We perform a comprehensive study of the right-handed neutrino parameter space and impose the correct observed relic density and SM neutrino mass differences and mixings. We find that the DM masses are in agreement with bounds from big-bang nucleosynthesis, but that these constraints induce sizeable DM couplings to the charged SM leptons. We then point out that previously overlooked limits from current and future lepton flavour violation experiments such as MEG and SINDRUM heavily constrain the allowed parameter space. Since the DM is leptophilic, we also investigate electron recoil as a possible direct detection signal, in particular in the XENON1T experiment. We find that despite the large coupling and low backgrounds, the energy thresholds are still too high and the predicted cross sections too low due to the heavy charged mediator, whose mass is constrained by LEP limits.

KEYWORDS: Dark matter, neutrino masses, direct detection, lepton flavour violation

Contents

1	Introduction	1
2	The SLIM model with MeV neutrino DM	3
2.1	Particle content	3
2.2	Lagrangian	3
2.3	Scalar masses and mixings after electroweak symmetry breaking	4
3	Collider, cosmological and neutrino constraints	4
3.1	Collider constraints	5
3.2	Cosmological constraints	6
3.3	Neutrino constraints	6
4	Right-handed neutrino DM relic density, mass and lepton couplings	8
5	Lepton flavour violation and experimental constraints	9
6	Electron recoil cross section and experimental sensitivity	12
6.1	Theoretical expectations	14
6.2	Experimental sensitivity	15
7	Conclusion	18

1 Introduction

While there is overwhelming evidence from many different length scales for the existence of dark matter (DM) in the Universe, its nature is still an unsolved problem in astroparticle physics [1]. Weakly Interacting Massive Particles (WIMPs) are very promising candidates, since – for masses in the GeV to TeV range and electroweak coupling strength – they lead in a straightforward way to the correct DM relic density. The latter has now been measured by Planck with the very high accuracy $\Omega h^2 = 0.1186 \pm 0.0020$, where h denotes the present Hubble expansion rate H_0 in units of $100 \text{ km s}^{-1} \text{ Mpc}^{-1}$ [2].

For many years, the lightest supersymmetric (SUSY) particle, the lightest neutralino, stabilised by a discrete R -parity symmetry, has been favoured, since there exist many other theoretical motivations for SUSY [3]. The neutralino relic density [4–6], direct detection [7] and LHC production cross sections [8] can even be computed with a precision that rivals the experimental one. However, neither the leading direct detection experiment in this mass range, XENON1T [9], nor the LHC [10] have so far produced any evidence for SUSY DM. In contrast, the discovery of a scalar boson of mass 125 GeV, consistent with the properties of the Standard Model (SM) Higgs boson, by ATLAS [11] and CMS [12] may imply the

existence of other scalars in Nature. When stabilised by a discrete Z_2 symmetry similar to R -parity, the lightest neutral eigenstate may well be the DM particle, as is the case *e.g.* in the inert doublet model [13–15].

In addition to the evidence for DM, the observed solar and atmospheric neutrino mass differences of $(7.59 \pm 0.20) \cdot 10^{-5} \text{ eV}^2$ and $(2.43 \pm 0.13) \cdot 10^{-3} \text{ eV}^2$ [16] require physics beyond the SM. Adding right-handed neutrinos to the SM has the advantage that they do not only allow for neutrino mass generation through different variants of the seesaw mechanism, but that they also help to restore parity at higher energy. If the seesaw mechanism is furthermore realised at one loop, DM and neutrino masses become closely related as *e.g.* in the scotogenic model [17] or variants thereof [18, 19]. The detection prospects of DM depend not only on its spin and other quantum numbers, but also strongly on its mass. While the observed large scale structure of the Universe has long been believed to favour the GeV to TeV cold DM regime [20], warm DM, and in particular keV sterile neutrinos, seem to account better for missing satellite galaxies, the cusp-core problem of inner DM density profiles and the too-big-to fail problem, *i.e.* the unobserved satellites are too big to not have visible stars [21]. Surprisingly, the MeV to GeV mass regime has so far remained largely unexplored.

Notable exceptions are variants of the SLIM (Scalar as Light as MeV) model, in which the SM is augmented at low energy by a scalar singlet and right-handed neutrinos [22] and in addition at higher energy *e.g.* by a complex doublet [23]. Original motivation for this model came from the fact that it could explain the 511 keV emission line from the centre of our galaxy, observed by the INTEGRAL satellite [24]. If the scalar singlet is complex and almost as light as the lightest sterile neutrino of MeV mass, the latter can be the DM and not only lead approximately to the correct DM relic density and active neutrino masses, but also solve the missing satellite and too-big-to-fail problems [25]. In addition to structure formation constraints, this variant of the SLIM model has also passed collider constraints from LEP and the LHC, that we will review below, and is thus not only very well motivated, but also worthy of further investigation.

In this paper, we impose for the first time the precise Planck measurement of the DM relic density as well as the neutrino mass differences and mixing angles through the Casas-Ibarra parametrisation. In addition, we study in detail the most competitive lepton flavour violation constraints that had so far been overlooked in the literature, but turn out to be highly restrictive on the allowed parameter space due to the fact that the scalar doublet couples also to the charged leptons [26]. Since the DM is light and leptophilic, *i.e.* has no tree-level couplings to quarks, no visible signal from nuclear recoils is expected, although the latter might well be induced at one loop for GeV to TeV DM masses [27]. We therefore study instead the electron recoil signal, which has recently come into focus for sub-GeV DM [28, 29] and should not only be sensitive to vector bosons (dark photons), but also other mediators, in particular the scalar doublet.

The goals of this paper are therefore threefold: First, after (re)defining the SLIM model with MeV neutrino DM in Sec. 2 and reviewing in Sec. 3 the theoretical and experimental constraints imposed previously, we calculate in Sec. 4 the precise DM relic density from neutrino mass difference and mixing constraints without any analytic approximations. The

result is not only the confirmation that neutrino DM is indeed viable in the MeV to GeV mass range, but also the prediction that its coupling to the scalar doublet can be large. Second, we compute in Sec. 5 the expected lepton flavour violation signals in the most sensitive channels $\mu \rightarrow e\gamma$, $\mu \rightarrow 3e$ and $\mu^- \text{Ti} \rightarrow e^- \text{Ti}$ and compare them with the sensitivities of current and future experiments. Third, we compute in Sec. 6 the resulting electron recoil cross section and compare it with new, realistic estimates of the XENON sensitivity and other experiments under preparation. In Sec. 7 we summarise our findings and discuss their generalisation to other models with MeV-scale DM.

2 The SLIM model with MeV neutrino DM

2.1 Particle content

In the SLIM model, the SM scalar (Higgs) doublet Φ with mass parameter m_1 , self-coupling λ_1 , squared vacuum expectation value (VEV) $v^2 = -2m_1^2/\lambda_1 = (246 \text{ GeV})^2$ and physical Higgs boson mass $m_h^2 = \lambda_1 v^2 = (125 \text{ GeV})^2$ is augmented at low energy by a real or complex scalar singlet. While both options are in principle possible, we will discuss later the phenomenological advantages of our choice of a complex scalar

$$\rho = \frac{1}{\sqrt{2}}(\rho_R + i\rho_I) \quad (2.1)$$

and (at least) two generations of singlet right-handed neutrinos N_i in order to effectively explain the observed DM and two non-zero neutrino masses at one loop [22]. The electroweak symmetry $SU(2)_L$ is restored at higher energy by the addition of a complex scalar doublet [23]

$$\eta = \begin{pmatrix} \eta^+ \\ \frac{1}{\sqrt{2}}(\eta_R + i\eta_I) \end{pmatrix}. \quad (2.2)$$

All new particles are stabilised by a global $U(1)$ symmetry that is softly broken to Z_2 . At variance with the original scotogenic model, which was directly based on the Z_2 symmetry and contained only the complex scalar doublet and the right-handed neutrinos [17], the soft breaking of $U(1)$ and the mixing of the scalar singlet and the neutral components of the scalar doublet, which both do not obtain a VEV, allow for MeV neutrino DM and two similarly light neutral scalars and thus for a solution to the missing satellite and too-big-to-fail problems [25]. In the classification of Ref. [18], the scotogenic and SLIM models correspond to models T3-B and T1-1-A with hypercharge parameters $\alpha = -1$ and 0, respectively.

2.2 Lagrangian

In the mass basis of the right-handed Majorana neutrinos N_i ($i = 1, 2$) and denoting the left-handed SM lepton flavour doublets as L_j ($j = 1, 2, 3$), the Higgs potential and additional terms in the Lagrangian are given by [23, 25]

$$\begin{aligned} \mathcal{L} = & -m_1^2 \Phi^\dagger \Phi - m_2^2 \eta^\dagger \eta - m_3^2 \rho^* \rho - \frac{1}{2} m_4^2 (\rho^2 + (\rho^*)^2) - \mu (\eta^\dagger \Phi \rho + h.c.) - \frac{1}{2} m_{N_i} \overline{N}_i^c N_i \\ & - \frac{1}{2} \lambda_1 (\Phi^\dagger \Phi)^2 - \frac{1}{2} \lambda_2 (\eta^\dagger \eta)^2 - \frac{1}{2} \lambda_3 (\rho^* \rho)^2 - \lambda_4 (\eta^\dagger \eta) (\Phi^\dagger \Phi) - \lambda_5 (\eta^\dagger \Phi) (\Phi^\dagger \eta) \\ & - \lambda_6 (\rho^* \rho) (\Phi^\dagger \Phi) - \lambda_7 (\rho^* \rho) (\eta^\dagger \eta) - (\lambda_8)_{ij} (\overline{N}_i^c \eta^\dagger L_j + h.c.). \end{aligned} \quad (2.3)$$

This DM model is leptophilic, as can be seen from the last term involving the couplings λ_8 , and remains renormalisable despite the soft breaking of the global $U(1)$ to Z_2 , which implies that m_4 should be small.

2.3 Scalar masses and mixings after electroweak symmetry breaking

After electroweak symmetry breaking, the charged components of the scalar doublet obtain the mass

$$m_{\eta^\pm}^2 = m_2^2 + \frac{1}{2}\lambda_4 v^2. \quad (2.4)$$

Due to the trilinear coupling μ , the neutral components of the complex singlet and doublet mix, and one obtains the mass matrix

$$M_{R,I}^2 = \begin{pmatrix} m_2^2 + (\lambda_4 + \lambda_5)\frac{v^2}{2} & \mu\frac{v}{\sqrt{2}} \\ \mu\frac{v}{\sqrt{2}} & m_3^2 + \lambda_6\frac{v^2}{2} \pm m_4^2 \end{pmatrix} =: \begin{pmatrix} A & B \\ B & C_{R,I} \end{pmatrix} \quad (2.5)$$

with a positive (negative) sign of the m_4^2 term for the real (imaginary) components. This leads to a very small mass splitting between the real and imaginary scalar mass eigenstates

$$\begin{pmatrix} \zeta_{1R,I} \\ \zeta_{2R,I} \end{pmatrix} = \begin{pmatrix} \cos\theta_{R,I} & -\sin\theta_{R,I} \\ \sin\theta_{R,I} & \cos\theta_{R,I} \end{pmatrix} \begin{pmatrix} \eta_{R,I} \\ \rho_{R,I} \end{pmatrix}, \quad (2.6)$$

which are obtained by rotation about the angles $\theta_{R,I}$. The eigenvalues of the mass matrix are given by

$$m_{R,I}^2 = \frac{1}{2} \left(A + C_{R,I} \pm \sqrt{(A - C_{R,I})^2 + 4B^2} \right). \quad (2.7)$$

Setting B^2 close to $AC_{R,I}$ with only a small difference

$$AC_{R,I} - B^2 =: \epsilon(A + C_{R,I}) \quad (2.8)$$

then allows to obtain two MeV neutral scalar mass eigenvalues ($m_{\zeta_{2R,I}}$), while the two others ($m_{\zeta_{1R,I}}$) will be of the same size as or larger than m_{η^\pm} .

3 Collider, cosmological and neutrino constraints

Although the SLIM model spans a relatively large parameter space, the latter turns out to be restricted significantly both theoretically and experimentally. Starting with the Higgs potential, both of its parameters (m_1 and λ_1) are now fixed by the known values of v and m_h (see Sec. 2.1). Theoretically, unitarity requires certain combinations of the couplings λ_k ($k = 2, \dots, 8$) to lie below 8π , while vacuum stability and the need to avoid tachyonic particles require others to be positive or larger than certain squared mass differences. These theoretical constraints turn out to be almost automatically satisfied, once collider and cosmological constraints are imposed. Several mass parameters (in particular $m_{2,3}$) then also directly depend on some of the couplings ($\lambda_{4,5,6}$). An overview of all model parameters, as defined by the Lagrangian in Eq. (2.3), together with their values or scan ranges and phenomenological impact is given in Tab. 1. They are described in detail in the following.

Table 1. Overview of model parameters with their values or scan ranges and phenomenological impact, respectively.

Parameter	Value	Range	Phenomenological impact
m_1^2	$-(89 \text{ GeV})^2$	–	Fixed by v and m_h
m_2	83 GeV	–	Fixed by v , λ_4 and λ_5
m_3	264 GeV	–	Fixed by v and λ_6
m_4	–	10 keV ... 10 MeV	Induces soft $U(1)$ breaking
μ	–	251 GeV ... 252 GeV	Fixed by v and ϵ
ϵ	–	$(10^{-5} \dots 6.1 \cdot 10^1) \text{ GeV}^2$	Induces MeV masses
m_{N_1}	–	$(0.1 \dots 0.98) \cdot m_{\zeta_2}$	$\mathcal{O}(\text{MeV})$ DM candidate
m_{N_2}	–	10 GeV ... 200 GeV	$\mathcal{O}(\text{GeV})$ sterile neutrino
λ_1	0.26	–	Fixed by v and m_h
λ_2	0.12	–	Induces only scalar conversions
λ_3	0.13	–	Induces only scalar conversions
λ_4	0.097	–	Fixed by v , $m_{\eta^\pm} = 99 \text{ GeV}$, $R_{\gamma\gamma}$
λ_5	0.13	–	Fixed by v , $m_{\eta^\pm} = 99 \text{ GeV}$, $R_{\gamma\gamma}$
λ_6	2.3	–	Induces MeV masses
λ_7	0.17	–	Induces only scalar conversions
λ_8	–	$10^{-6} \dots 10^2$	Fixed by Casas-Ibarra parametr.

3.1 Collider constraints

The SM scalar Higgs doublet Φ couples to the new complex scalar doublet η and singlet ρ through the matrix

$$\begin{pmatrix} \eta \\ \rho \end{pmatrix}^\dagger \begin{pmatrix} (\lambda_4 + \lambda_5)v & \frac{\mu}{\sqrt{2}} \\ \frac{\mu}{\sqrt{2}} & \lambda_6 v \end{pmatrix} \Phi \begin{pmatrix} \eta \\ \rho \end{pmatrix}. \quad (3.1)$$

Inspection of Eq. (2.5) shows that, for negligibly small m_4 , the identifications [25]

$$m_2^2 = (\lambda_4 + \lambda_5) \frac{v^2}{2} \quad \text{and} \quad m_3^2 = \lambda_6 \frac{v^2}{2} \quad (3.2)$$

make the Higgs coupling matrix proportional to the scalar mass matrix. While the invisible decays $h \rightarrow \zeta_{1R,I} \zeta_{1R,I}$ can be forbidden by choosing $m_{\zeta_{1R,I}} > m_h/2$, the decays $h \rightarrow \zeta_{2R,I} \zeta_{2R,I} \rightarrow N_1 N_1 \nu \nu$ will generally be kinematically open due to the small values of $m_{\zeta_{2R,I}}$, but then also have negligible branching ratios. As a consequence, $m_{2,3}$ are fixed by $\lambda_{4,5,6}$. Experimentally, the current ATLAS and CMS limits on the invisible Higgs branching ratio lie at 26% and 19%, respectively [30, 31].

A linear combination of the parameters $\lambda_{4,5}$ can in turn be restricted by observing that the charged scalar mass m_{η^\pm} in Eq. (2.4) must lie above the rather model-independent LEP limit of 98.5 GeV for charged scalars [32]. The charged scalar also contributes to the Higgs branching ratio into two photons, for which CMS now measures a ratio to the SM value of $R_{\gamma\gamma} = 1.20_{-0.14}^{+0.18}$ [33]. Choosing $\lambda_{4,5} \simeq 0.1$ ($\lambda_4 = 0.097$, $\lambda_5 = 0.13$) satisfies both constraints, as we have verified and can also be seen from Fig. 3 in Ref. [25]. Larger values

of λ_4 would lead to larger m_{η^\pm} and thus smaller electron recoil cross sections and lepton flavour violation, while λ_5 has similar, but somewhat less phenomenological influence.

3.2 Cosmological constraints

Although studies of the SLIM model initially focused on the possibility of *scalar* MeV DM [22, 23], also to explain the 511 keV line from the galactic centre [24], it was later noticed that the problems of missing satellite galaxies, the cusp core of inner DM density profiles and the fact that the unobserved satellites are too big to not have visible stars [21] can rather be solved with MeV *neutrino* DM, provided that it scatters off the active neutrinos in the early Universe by exchanging only slightly heavier scalars [25].

In the scalar sector, these cosmological constraints translate into singlet and doublet mass parameters that should be close to each other, so that the cancellation described in Sec. 2.3 can occur. While $\lambda_{2,3,7}$ only control the scalar potentials and the conversion of scalars into each other with little influence on the phenomenology (we take *e.g.* $\lambda_2 = 0.12$, $\lambda_3 = 0.13$, and $\lambda_7 = 0.17$), the singlet mass parameter m_3 should not be much larger than v (*i.e.* $\lambda_6 \leq 3$), as was also observed in Fig. 2 of Ref. [25]. Instead of varying λ_6 and fixing ϵ to 10^{-4} GeV², we rather fix $\lambda_6 = 2.3$ and vary the mass splitting parameter in Eq. (2.8)

$$\epsilon = (10^{-5} \dots 6.1 \cdot 10^1) \text{ GeV}^2. \quad (3.3)$$

This has the advantage of more directly controlling the off-diagonal mass parameter μ and thus the MeV mass of the two light scalars $\zeta_{2R,I}$.

It has been shown in Refs. [34, 35] that weak-strength DM interactions can erase the DM primordial fluctuations when the DM is relatively light (of $\mathcal{O}(\text{MeV})$) and coupled to neutrinos or photons. The elastic scattering cross section must then, however, be temperature-independent, which requires, in addition to MeV DM mass and weak-strength DM couplings, a small mass splitting of the MeV neutrino DM and the lightest scalar. This is ensured in all our scenarios through the imposed scan ranges, in particular of m_4 , ϵ and λ_6 .

For the lighter Majorana neutrino N_1 to represent DM and solve the cosmological problems, it must therefore be (only somewhat) lighter than the lightest scalar. We therefore vary $m_{N_1}/m_{\zeta_{2R,I}}$ in the range 0.1 ... 0.98. In contrast, when the second Majorana neutrino N_2 is heavy (10 GeV ... 200 GeV, the exact value being constrained by the active neutrino mass differences and mixings), it decays promptly through $N_2 \rightarrow \eta\nu \rightarrow N_1\nu\nu$ and contributes neither significantly to the relic density nor to any other signal considered here. A third Majorana neutrino could of course be added, but would not significantly change the phenomenology.

3.3 Neutrino constraints

In radiative seesaw models, the neutrinos obtain their masses only at the loop level, and in particular in the SLIM model through the one-loop diagram shown in Fig. 1.

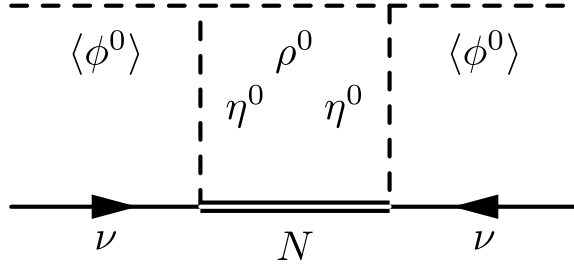


Figure 1. One-loop diagram leading to the active neutrino mass matrix in the SLIM model.

Taking the mixing in the neutral scalar sector as described in Sec. 2.3 into account, the neutrino mass matrix is given by [25]

$$(M_\nu)_{ij} = \sum_k \frac{(\lambda_8)_{ik}(\lambda_8)_{jk}}{16\pi^2} m_{N_k} \left[\frac{\cos^2 \theta_R m_{1R}^2}{m_{1R}^2 - m_{N_k}^2} \ln \frac{m_{1R}^2}{m_{N_k}^2} + \frac{\sin^2 \theta_R m_{2R}^2}{m_{2R}^2 - m_{N_k}^2} \ln \frac{m_{2R}^2}{m_{N_k}^2} - \frac{\cos^2 \theta_I m_{1I}^2}{m_{1I}^2 - m_{N_k}^2} \ln \frac{m_{1I}^2}{m_{N_k}^2} - \frac{\sin^2 \theta_I m_{2I}^2}{m_{2I}^2 - m_{N_k}^2} \ln \frac{m_{2I}^2}{m_{N_k}^2} \right]. \quad (3.4)$$

As in the scotogenic model, the neutrino masses arise from the small mass differences between the real and imaginary scalars. In the SLIM model, this mass splitting is realised by the non-zero value of m_4 (cf. Sec. 2.3), required to be small from the soft breaking of $U(1)$ to Z_2 . We do not fix m_4 here to the relatively large value of 3 MeV as in Ref. [25], but allow it to vary in the range 10 keV ... 10 MeV, as a smaller mass splitting of $\zeta_{2R,I}$ reduces the mass-dependent terms in the neutrino mass matrix and thus indirectly allows for larger lepton couplings λ_8 .

We take the neutrino mass and mixing constraints into account assuming for simplicity a massless lightest neutrino, which implies a normal hierarchy and absolute values for the other two neutrino masses in the mass matrix

$$D_\nu = U_\nu^\dagger M_\nu U_\nu = \text{diag}(0, m_{\nu 2}, m_{\nu 3}), \quad (3.5)$$

diagonalised by the PMNS matrix U_ν .

To impose the experimental constraints on the neutrino mass and mixing, we make use of the Casas-Ibarra parametrisation [36]. It takes as an input the experimental neutrino data and the dark particle masses and mixings and returns the coupling λ_8 . Specifically, we rewrite Eq. (3.4) as

$$M_\nu = \lambda_8^T M \lambda_8, \quad (3.6)$$

where M is a 3×3 diagonal matrix whose elements are differences of mass functions, summed over k . Together with Eq. (3.5) we then obtain

$$D_\nu = U_\nu^\dagger \lambda_8^T M \lambda_8 U_\nu \quad (3.7)$$

or

$$\text{diag}(0, 1, 1) = D_\nu^{-1/2} U_\nu^\dagger \lambda_8^T M \lambda_8 U_\nu D_\nu^{-1/2} \equiv R^\dagger R, \quad (3.8)$$

where the rotation angle θ in

$$R = \begin{pmatrix} 0 & \cos \theta & \sin \theta \\ 0 & -\sin \theta & \cos \theta \end{pmatrix} \quad (3.9)$$

is arbitrary, *i.e.* it can vary in the range $0 \dots 2\pi$. Identifying

$$R = M^{1/2} \lambda_8 U_\nu D_\nu^{-1/2} \quad (3.10)$$

then leads to the desired couplings

$$\lambda_8 = M^{-1/2} R D_\nu^{1/2} U_\nu^\dagger, \quad (3.11)$$

that are consistent with the neutrino data and depend not only on θ , but also indirectly on the scalar and right-handed neutrino masses as well as the scalar couplings in the potential. The coupling λ_8 itself determines many properties of the model. Apart from being responsible for the neutrino masses, it also directly influences the relic density, the electron recoil cross section, as well as the amplitude of lepton flavour violating processes such as $\mu \rightarrow e\gamma$.

4 Right-handed neutrino DM relic density, mass and lepton couplings

We now come to the first new result of our study, *i.e.* a numerical calculation of the precise right-handed neutrino DM relic density without any analytic approximations. To this end, we reproduce the Lagrangian of the SLIM model [23, 25] presented in Eq. (2.3) from the particle content defined in Sec. 2.1 using our program MINIMAL-LAGRANGIANS [37]. The corresponding Feynman rules are then derived with SARAH 4.14.2 [38] and passed on to SPHENO 4.0.3 [39] to calculate the physical mass spectrum for each point in the parameter space that we have defined in Sec. 3.

At this point, we do not only impose the collider, cosmological and neutrino constraints in the ways described there, but also use SPHENO 4.0.3 to check (again) other collider and low-energy constraints such as the Z and Higgs boson branching ratios, the ρ parameter, and the braching ratio of the flavour-changing neutral current process $b \rightarrow s\gamma$. The right-handed neutrino DM relic density for each surviving model is then calculated with MICROMEGAS 4.3.5 [40].

Figure 2 shows the DM relic density Ωh^2 of all viable SLIM models with right-handed neutrino DM versus the absolute value of its coupling to electrons and electron neutrinos λ_8^{e1} , coloured according to the value of the mass m_{N_1} of the DM candidate. One can clearly see that the relic density drops quickly from 10^0 to 10^{-4} when the lepton coupling rises by about two orders of magnitude, *e.g.* from a few times 10^{-4} to 10^{-2} or 10^{-2} to a few times 10^{-1} . However, the correct relic density as observed by Planck (blue horizontal band) [2] can be obtained for all couplings in these ranges, provided that the DM mass rises simultaneously from the MeV (dark blue) to the GeV scale (light green/yellow). We have therefore confirmed that while MeV dark matter is indeed consistent with collider, structure formation and neutrino constraints, the correct relic density imposes further restrictions and

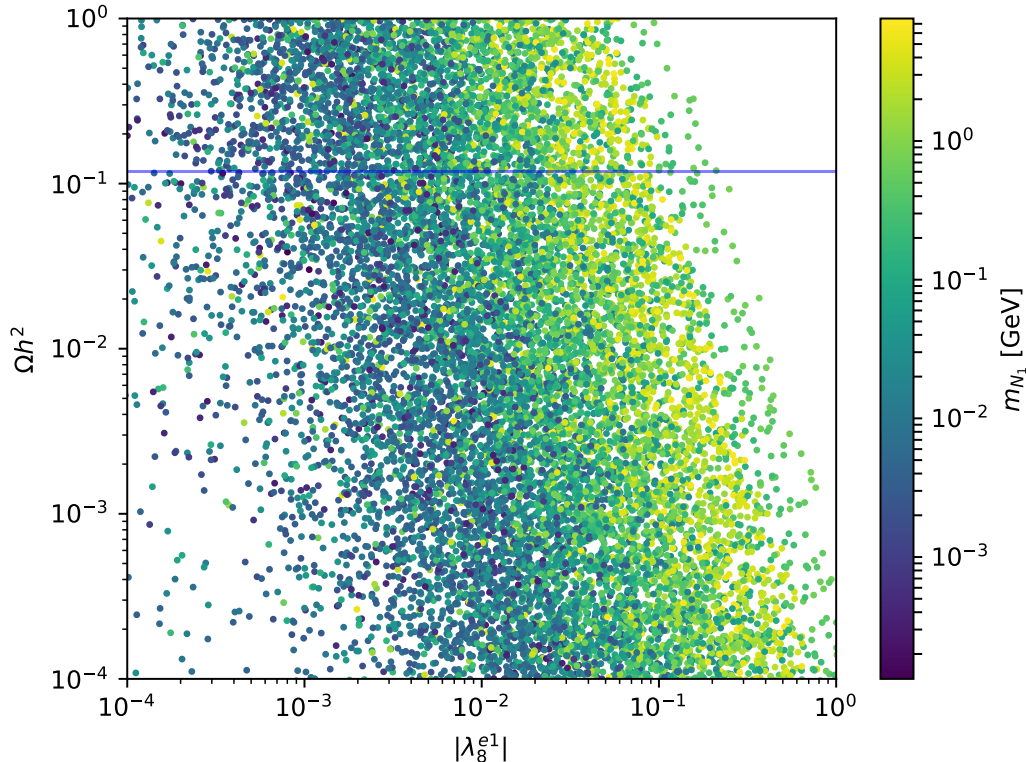


Figure 2. The relic density Ωh^2 obtained in the SLIM model with right-handed neutrino DM versus the absolute value of its coupling to electrons and electron neutrinos λ_8^{e1} . The relic density measured by Planck [2] is shown as a blue horizontal band, and the lightest Majorana neutrino mass m_{N_1} is given on a colour scale.

in fact predicts sizeable couplings of almost up to $\mathcal{O}(1)$ to the SM leptons. In the following, we therefore impose also the Planck value for the relic density.

In Fig. 3 we show all models, which satisfy not only collider, cosmological and neutrino mass constraints, but also lead to the correct relic density. It therefore represents a projection of Fig. 2 on the blue line and is displayed in the plane of the absolute value of the DM-electron coupling $|\lambda_8^{e1}|$ versus DM mass m_{N_1} . As one can observe, heavier DM implies enhanced DM annihilation processes through larger couplings to the SM leptons in order to reduce the DM abundance and still obtain the correct relic density.

5 Lepton flavour violation and experimental constraints

Since the right-handed neutrinos N_i in our model couple through the complex scalar doublet η not only to SM neutrinos, but also to the charged leptons, processes that violate lepton flavour naturally occur at the one-loop level. The most sensitive process with the strictest experimental bounds is usually the flavour-changing neutral current process $\mu \rightarrow e\gamma$. Here, it occurs through the Feynman diagrams shown in Fig. 4 and depends, apart from the

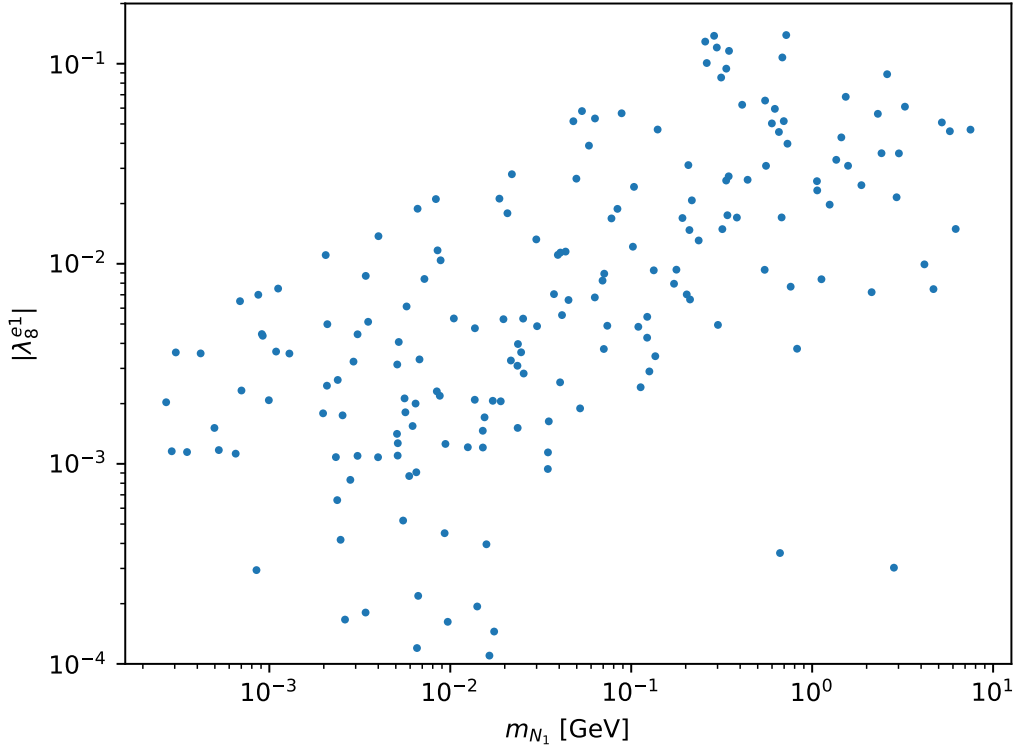


Figure 3. DM-electron coupling λ_g^{e1} versus DM mass m_{N_1} for models which satisfy not only collider, cosmological and neutrino mass constraints, but also lead to the correct relic density.

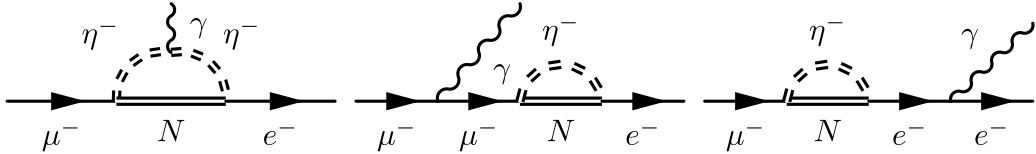


Figure 4. Feynman diagrams contributing to the lepton flavour violating process $\mu \rightarrow e\gamma$ at one loop through the exchange of Z_2 -odd right-handed neutrinos (N) and charged scalars (η^-).

exchanged particle masses, not only on the couplings λ_g^{ei} , but also on $\lambda_g^{\mu i}$, which are both constrained by the neutrino masses and mixings through the Casas-Ibarra parametrisation.

We compute the branching ratio of the process $\mu \rightarrow e\gamma$ with SPHENO 4.0.3 [39] and plot it in Fig. 5 as a function of the dominating couplings λ_g^{e1} on the x -axis and $\lambda_g^{\mu 1}$ on a colour scale. Interestingly, the non-zero neutrino masses impose a lower bound on this branching ratio of about 10^{-17} . Experimentally, the MEG experiment currently excludes branching ratios above $4.2 \cdot 10^{-13}$ [41]. This already excludes a substantial part of the parameter space and in particular couplings λ_g^{e1} above $6 \cdot 10^{-3}$ and $\lambda_g^{\mu 1}$ above about 10^{-2} . In the SLIM model with scalar DM, similar limits of a few times 10^{-3} and a few times 10^{-2} , respectively, have

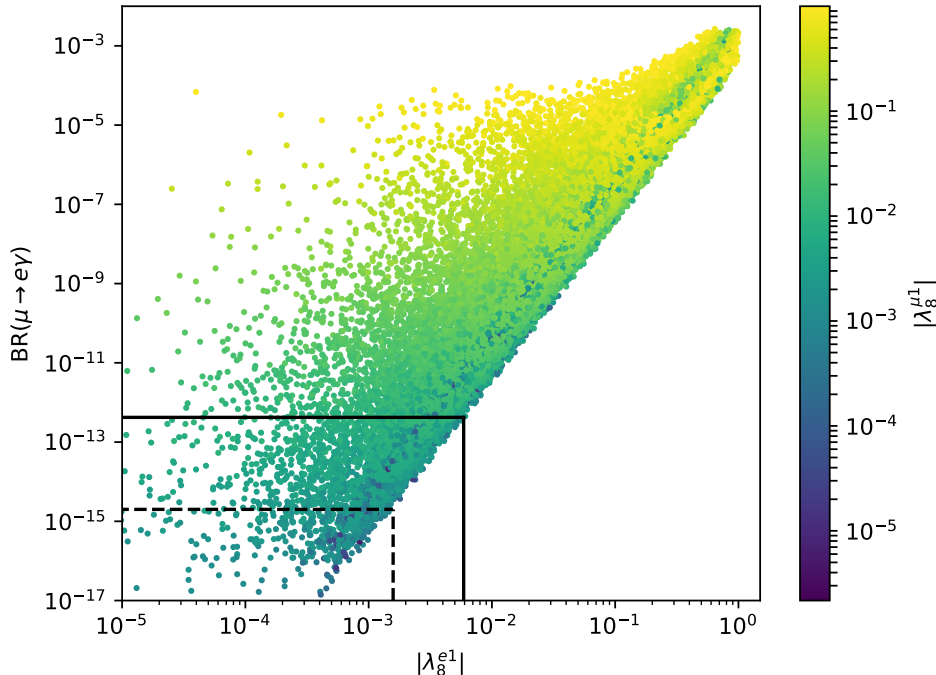


Figure 5. Branching ratio of the lepton flavour violating process $\mu \rightarrow e\gamma$ versus the DM-electron coupling λ_8^{e1} . The DM-muon coupling $\lambda_8^{\mu 1}$ is shown on a colour scale. Also shown are the current (solid black line) [41] and expected future (dashed black line) [42] limits on the branching ratio by the MEG experiment.

been expected in an approximate calculation [23]. After the planned upgrade of the MEG experiment, it is expected to reach a sensitivity of $2 \cdot 10^{-15}$ [42], which would lower the limits on the couplings by about a factor of four, leaving open only a small part of the parameter space.

The current limit on the branching ratio $\mu \rightarrow 3e$ obtained by the SINDRUM experiment lies at 10^{-12} [43]. It is thus only slightly weaker than the MEG limit on $\mu \rightarrow e\gamma$. In addition, SINDRUM II obtained a limit of $4.3 \cdot 10^{-12}$ on the muon-to-electron conversion rate in Titanium [44]. Significant progress is expected for both processes with possible future limits of 10^{-16} [45] and even 10^{-18} [46], respectively. In Fig. 6 we therefore show predictions for these processes in our viable models, satisfying all collider, cosmological and neutrino constraints, together with those for $\mu \rightarrow e\gamma$ and compare them to the current (solid lines) and future (dashed lines) experimental limits. We observe a strong correlation of all three processes, except for large, already excluded branching ratios and conversion rates. While the current limit on $\mu \rightarrow e\gamma$ sets the strongest bound, the other two experiments will indeed reach a similar sensitivity in the future. Note that the scans in Figs. 5 and 6 do not include the constraint on the correct relic density, i.e. also points which under- (or over-) saturate the relic density are included.

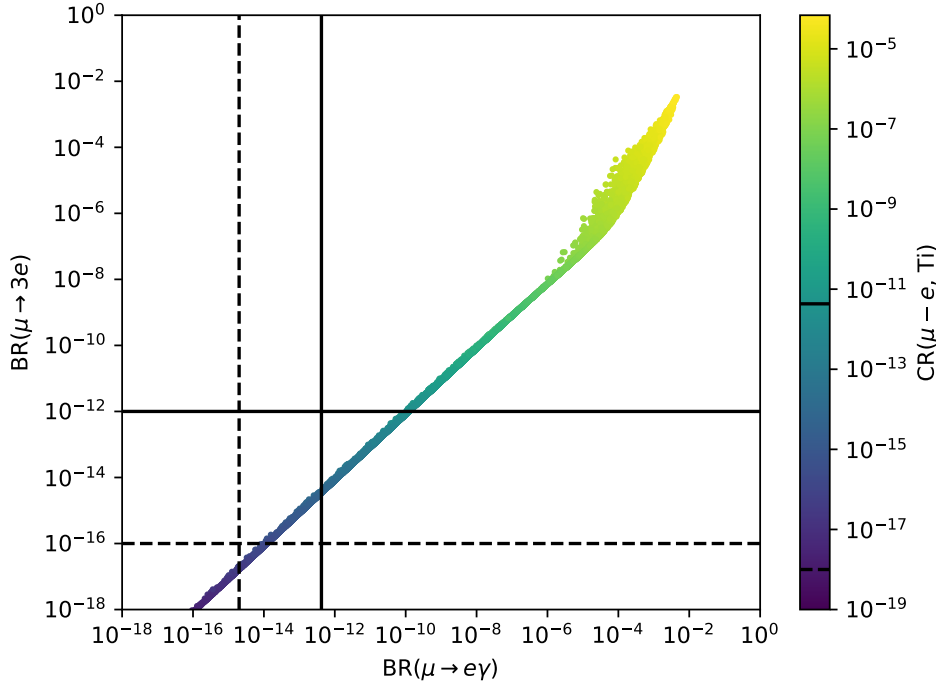


Figure 6. Branching ratio of the lepton flavour violating process $\mu \rightarrow 3e$ versus the one of the (usually most constraining) process $\mu \rightarrow e\gamma$. The rate of muon conversion in the field of titanium atoms $\mu^- \text{Ti} \rightarrow e^- \text{Ti}$ is shown on a colour scale. Also shown are the current (solid black lines) [41, 43, 44] and expected future (dashed black lines) [42, 45, 46] experimental limits on the branching ratios and conversion rate.

6 Electron recoil cross section and experimental sensitivity

As described in the introduction, the DM in the SLIM model is leptophilic, so that one does not expect any nuclear recoil signal from experiments like XENON1T, which has set the current best limit on the spin-independent direct detection cross section for DM masses between 6 GeV and 1 TeV [9], XENON100, which had extended the sensitivity down to 3.7 GeV using the ionisation (S2) signal only [47], or CRESST-III, whose cryogenic CaWO_4 crystals are even sensitive down to DM masses of 160 MeV [48].

Given that the DM is of MeV to GeV mass and its couplings to the SM leptons are large, one would, however, expect an observable electron recoil signal, which has recently come into focus for sub-GeV DM and should not only be sensitive to vector bosons (dark photons), but also other mediators [28, 29]. If we generalise the notation for the DM particle to the conventional χ , the ionisation rate, differential in the electron recoil (er) energy E_{er} ,

$$\frac{dR_{\text{ion}}}{d \ln E_{\text{er}}} = N_{\text{T}} \frac{\rho_{\chi}}{m_{\chi}} \sum_{n\ell} \frac{d\langle \sigma_{\text{ion}}^{n\ell} v \rangle}{d \ln E_{\text{er}}} \quad (6.1)$$

is proportional to the number of target nuclei per unit mass N_{T} , the local DM density

$\rho_\chi = 0.4 \text{ GeV/cm}^3$ [49], the differential thermally averaged cross section

$$\frac{d\langle\sigma_{\text{ion}}^{n\ell}v\rangle}{d\ln E_{\text{er}}} = \frac{\bar{\sigma}_{\chi e}}{8\mu_{\chi e}^2} \int |f_{\text{ion}}^{n\ell}(k', q)|^2 F(k', Z_{\text{eff}}) |F_{\text{DM}}(q)|^2 \eta(v_{\text{min}}, t) q dq, \quad (6.2)$$

summed over all possible electron states (n, ℓ) , and inversely proportional to the DM mass m_χ . In Eq. (6.2), $\mu_{\chi e}$ is the DM-electron reduced mass, and $k' = \sqrt{2m_e E_{\text{er}}}$ and q are the outgoing electron momentum and momentum transfer, respectively. Assuming plane waves for the scattered electrons and a spherically symmetric atom with full shells, the form factor for ionisation reduces to

$$\left|f_{\text{ion}}^{n\ell}(k', q)\right|^2 = \frac{(2\ell + 1)k'^2}{4\pi^3 q} \int |\chi_{n\ell}(k)|^2 k dk, \quad (6.3)$$

where $\chi_{n\ell}(k)$ is the radial part of the momentum space wave function of the bound electron [27]. As in the case of nuclear beta decay, the wave function of the escaping electron is distorted by the presence of the nearby atom, requiring that the rate be corrected by the Fermi function

$$F(k', Z_{\text{eff}}) = \frac{2\pi\nu}{1 - e^{-2\pi\nu}} \quad \text{with} \quad \nu = Z_{\text{eff}} \frac{\alpha m_e}{k'}. \quad (6.4)$$

Z_{eff} is the effective charge felt by the electron, expected to be somewhat larger than unity. However, for outer shell electrons $Z_{\text{eff}} = 1$ is a good approximation [28, 29]. Treating the electrons in the target as single-particle states of an isolated atom, we can use the tabulated numerical Roothaan-Hartree-Fock (RHF) wave functions [50]. Astrophysics enters through the mean inverse DM velocity [29]

$$\eta(v_{\text{min}}, t) = \int_{v_{\text{min}}}^{\infty} \frac{d^3v}{v} f(\mathbf{v}, t), \quad (6.5)$$

which depends on the Earth-frame velocity distribution of DM $f(\mathbf{v}, t)$, that acquires a time dependence as the Earth orbits the Sun. In the Galactic frame, and asymptotically far away from the Sun's gravitational potential, we take the velocity distribution $f_\infty(\mathbf{v})$ to be that of the Standard Halo Model

$$f_\infty(\mathbf{v}) = 1/N_{\text{esc}} (\pi v_0^2)^{-3/2} e^{-\mathbf{v}^2/v_0^2}, \quad \text{if} \quad |\mathbf{v}| \leq v_{\text{esc}}, \quad (6.6)$$

where N_{esc} is a normalisation factor. We adopt a local circular velocity of $v_0 = 220 \text{ km/s}$ and an escape velocity of $v_{\text{esc}} = 544 \text{ km/s}$ [51]. The minimal DM velocity

$$v_{\text{min}} = \frac{E_{\text{B}}^{n\ell} + E_{\text{er}}}{q} + \frac{q}{2m_\chi} \quad (6.7)$$

depends on the required sum of binding energy $E_{\text{B}}^{n\ell}$ and recoil energy E_{er} .

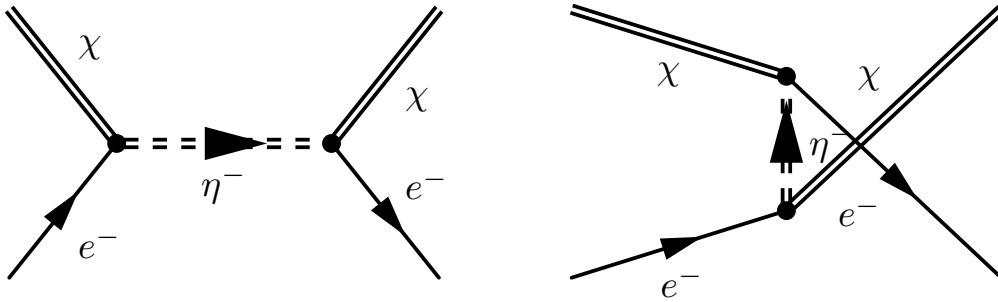


Figure 7. Feynman diagrams contributing to the scattering of right-handed neutrino DM ($\chi = N_1$) off electrons (e^-) through s - and u -channel exchanges of the charged Z_2 -odd scalars (η^-).

6.1 Theoretical expectations

In Eq. (6.2), we are of course primarily interested in the DM scattering cross section off electrons. It is usually factorised into the non-relativistic reference cross section

$$\bar{\sigma}_{\chi e} = \frac{\mu_{\chi e}^2}{16\pi m_\chi^2 m_e^2} \overline{|\mathcal{M}_{e\chi}(q)|^2} \Big|_{q^2=\alpha^2 m_e^2} \quad (6.8)$$

at fixed momentum transfer $q = \alpha m_e$, where α is the electromagnetic fine structure constant and m_e is the electron mass, and the form factor

$$|F_{\text{DM}}(q)|^2 = \overline{|\mathcal{M}_{e\chi}(q)|^2} / \overline{|\mathcal{M}_{e\chi}(\alpha m_e)|^2}, \quad (6.9)$$

that captures the q -dependence of the matrix element. For light mediators, $F_{\text{DM}}(q) = \alpha^2 m_e^2 / q^2$, whereas for heavy mediators $F_{\text{DM}}(q) = 1$. In our model, the DM particles χ are the right-handed neutrinos N_1 . They scatter off the electrons through the exchange of the Z_2 -odd scalars η^- , coupling with strength λ_8^{e1} , in the s - and u -channel, as shown in the Feynman diagrams in Fig. 7. Since the charged scalar η^- is heavy (cf. Sec. 3.2), the propagator can be integrated out with the result that the form factor $F_{\text{DM}}(q) = 1$ and the reference cross section is

$$\bar{\sigma}_{\chi e} = \frac{\mu_{\chi e}^2 (\lambda_8^{e1})^4}{\pi m_{\eta^\pm}^4}. \quad (6.10)$$

For the models satisfying all the constraints described in Sec. 3 and reproducing the observed DM relic density as described in Sec. 4, the numerical values of the scattering cross sections of right-handed neutrino DM off electrons are shown in Fig. 8 as a function of the DM mass. In addition, the size of the DM-electron coupling λ_8^{e1} is shown on a colour scale. The cross sections do not exceed a few times 10^{-46} cm² even for the largest couplings $\lambda_8^{e1} \geq 0.1$ and reach only 10^{-52} cm², when in addition the lepton flavour violation constraints of Sec. 5 are imposed. The reason is the strong suppression by the large mass m_{η^\pm} of the charged scalar mediator, which is constrained by the LEP limit to be heavier than 98.5 GeV (cf. Sec. 3.1) and which enters with the fourth power in Eq. (6.10). Note that most of our viable models have DM masses above a few MeV, which is in excellent agreement with bounds on big-bang nucleosynthesis (BBN) [52].

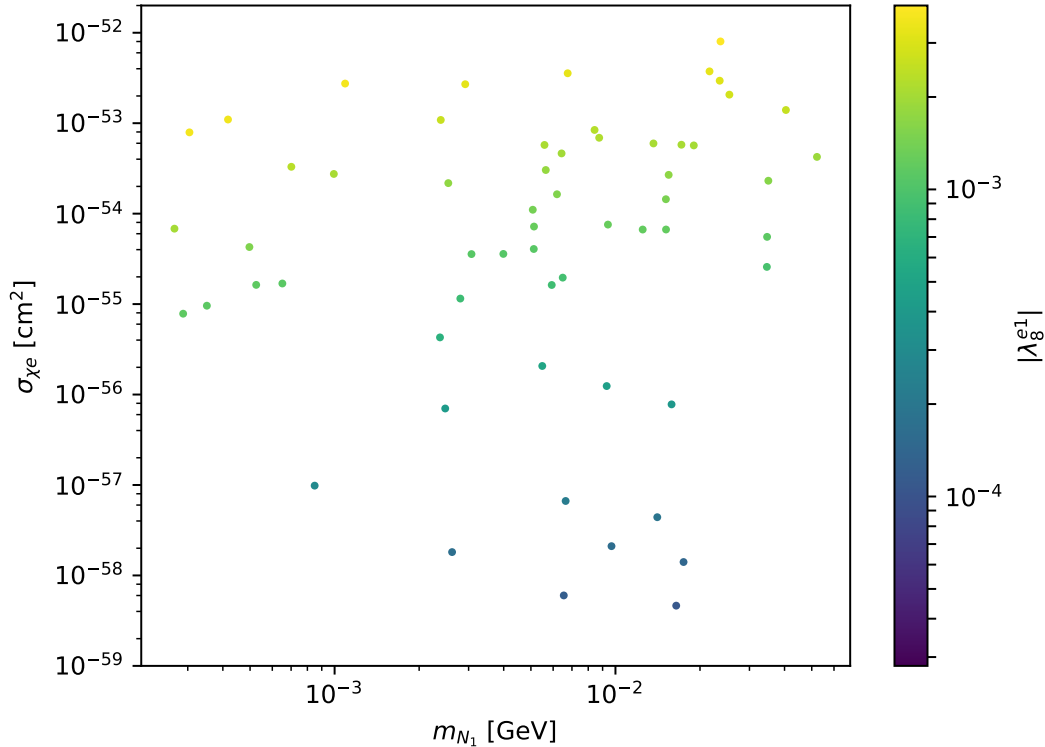


Figure 8. Scattering cross section of right-handed neutrino DM off electrons versus the DM mass. The DM-electron coupling λ_g^{e1} is shown on a colour scale.

6.2 Experimental sensitivity

For DM with sub-GeV mass and no nuclear interactions, direct detection experiments must rely on the recoil of (one or several) electrons leading to ionisation. The cross section sensitivity of an experiment with a liquid xenon (LXe) target and an exposure of 1 kg-year, assuming a constant form factor, no detector threshold and only the irreducible neutrino background, was initially estimated to be a few times 10^{-41} cm² for masses of a few tens of MeV [28]. In Fig. 9 we plot this sensitivity (red dotted line) for an exposure of 60 kg-year by simply scaling it down by a factor of 60, neglecting the influence of the tiny but non-zero irreducible background of neutrino scattering. We will see below that an exposure of 60 kg-year can be realistically achieved with present experiments. This sensitivity is, however, still ten orders of magnitude away from the cross section range shown in Fig. 8.

In the following, we investigate how realistic the assumptions of no detector energy threshold and only irreducible neutrino background for DM experiments with a LXe target are, taking the example of XENON1T with the so far largest LXe target. Its ultra-low background rate for electron recoils of 82_{-3}^{+5} events/(ton-year·keV) at low energies represents the lowest background level in the world for a DM experiment. It is achieved by a strict material selection w.r.t. radio-purity and by fiducialising an inner self-shielded LXe

volume. The interaction point is reconstructed by using both the scintillation light (S1) and the charge signal (S2). Unfortunately, demanding an S1 signal restricts the electron recoil energy to more than 2.5 (2.3) keV for XENON10 (XENON100) [53] and 1.3 keV for XENON1T [9]. These energies are significantly larger than the electron binding energy of a few tens of eV. First, we estimate the sensitivity of the XENON1T experiment for the 1 ton-year exposure collected for the spin-independent WIMP nuclear recoil analysis [9], using realistic backgrounds and energy thresholds and the standard mode of fiducialisation with both the S1 and S2 signals. As discussed in Ref. [54], the electron recoil background in XENON1T is expected to be flat in the region of interest (ROI) of the WIMP search and dominated by β -decays of the ^{214}Pb originating from ^{222}Rn emanations. The largest subdominant background comes from β -decays of ^{85}Kr , whose average natural concentration is reduced through cryogenic distillation down to the sub-ppt level [55]. The energy threshold is defined by a corrected scintillation (cS1) signal between 3 and 70 photoelectrons (PE) and an ionisation (S2) signal threshold of 200 PE [9]. Similarly to the procedure in Ref. [56], a conversion function between S1 in PE and energy recoil in keV can be derived by using the Noble Element Simulation Technique (NEST) [57]. As further discussed in Ref. [58], NEST contains a global analysis of LXe measurements from all available historical data for the mean photon and charge yield, including XENON1T. Thus, a reliable conversion down to the 1 keV energy threshold, where the detection efficiency of XENON1T drops to less than 10%, is available. Using the NEST conversion function, we explore both a conservative detection threshold of 2 keV, where a full triggered efficiency is still possible, and for illustration also 1 keV, where the detection efficiency is already limited. Using Poisson statistics (cf. Tab. XXII of Ref. [59]), we then obtain for each assumed DM mass an average upper limit on the event rate and thus the experimental sensitivity on the reference cross section $\bar{\sigma}_{\chi e}$ (green and blue lines in Fig. 9). In principle, the sensitivity can be improved by using the expected annual modulation of a DM signal in an earth-bound detector rotating once per year around the sun and thus possessing an annually modulated velocity w.r.t. to the DM wind. Using this time information, the XENON100 experiment with its electron energy threshold of 2.3 keV became sensitive to DM masses down to 600 MeV with a lowest cross section of $6 \cdot 10^{-35} \text{ cm}^2$ for a DM mass of 2 GeV and axial-vector couplings [60] (black line in Fig. 9).

To really come closer to the ideal sensitivity line, the energy threshold has to be lowered drastically by abandoning the scintillation light requirement S1 and using only the charge signal S2, which has a lower energy threshold. The disadvantage of this method is that fiducialisation is limited, since without S1 the event depth z cannot be accurately estimated, yielding a potentially increased background. Furthermore, there are additional single-electron backgrounds coming from the photoionisation of impurities of the LXe and the metal components inside the time-projection chamber [61], which are difficult to describe without considering the information provided by the scintillation light. Therefore, a reliable background model becomes difficult. With this method, searches for DM scattering off nuclei with XENON10 with a 1 keV nuclear recoil energy threshold and an exposure of 15 kg-days [62] as well as with XENON100 with a 0.7 keV nuclear recoil energy threshold and an exposure of 30 kg-years [47] have been performed, assuming very conservatively that

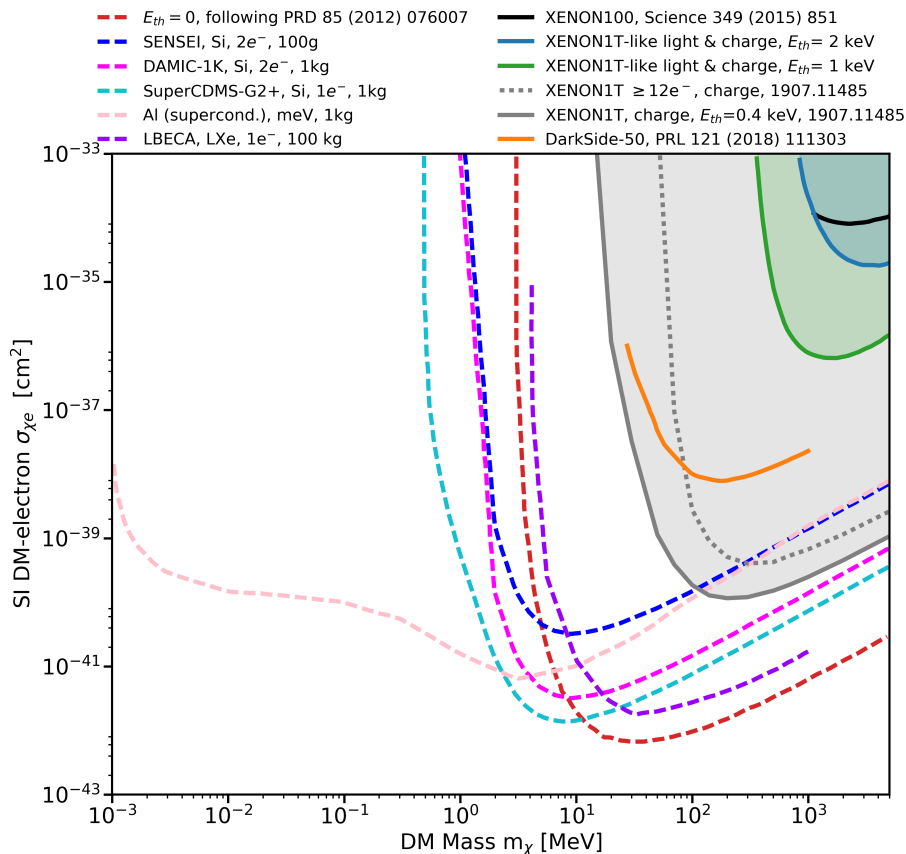


Figure 9. Experimental upper limits and estimated sensitivities for the DM-electron scattering cross section $\bar{\sigma}_{\chi_e}$ in LXe, LAr and other detectors. Shown are the previously estimated sensitivity for a 60 kg-year exposure assuming only irreducible neutrino backgrounds and no detection thresholds (red dotted) [28] together with our sensitivity estimates for an assumed electron energy detection threshold of 2 keV (blue) and 1 keV (green), respectively, for a 1 ton-year exposure of XENON1T with realistic assumptions at 95 % confidence level (C.L.) [9]. Also shown are published limits from XENON100 (black) [60] and a charge-only analysis of XENON1T [63] (gray full line), both at 90 % C.L. The gray dotted line is a more conservative version of the latter limit considering that electron recoils below 186 eV (12 produced electrons) are undetectable, as the LXe charge yield Q_y has never been measured below these energies [63]. For comparison, we also show the ionisation-only limit in Argon from DarkSide-50 (orange full line) [64] and sensitivity projections (dashed lines) for SENSEI (blue), DAMIC-1K (magenta), Al (supercond.) (pink), SuperCDMS (cyan) [65] and LBECA (purple) [66].

all counts in the search window are potential signal counts. In Ref. [28] these analyses were re-interpreted in terms of light DM scattering off electrons, and exclusion limits of $3 \cdot 10^{-38}$ cm^2 or just below 10^{-38} cm^2 at 100 MeV were obtained.

Very recently XENON1T published a S2-only analysis [63] with an electron energy threshold of 0.4 keV. Strict cuts on the data were applied to lower the background drastically down to 1 event/(ton \cdot day \cdot keV), resulting in a remaining effective exposure of 22 ton-days or 60 kg-years. The analysis considered a flat electron recoil background originating mainly

from ^{214}Pb decays, coherent elastic neutrino-nucleon scattering and “cathode events”, which were attributed to low energy β -electrons from the cathode wire grid. This analysis was sensitive to light DM scattering off electrons down to masses of 100 to 20 MeV (gray lines in Fig. 9).

Comparing the estimated sensitivities and experimental limits plotted in Fig. 9 to the reference cross section of at most a few times 10^{-52} cm² in the SLIM model in Fig. 8, we observe a difference of ten orders of magnitude despite the MeV to GeV DM mass and large electron couplings. The reason is of course the large suppression by the fourth power in the mass of the charged heavy mediator. Despite the fact that XENON1T has demonstrated unprecedented low background levels, the exclusion reach is still heavily constrained by the detection threshold. Skipping the requirement to detect the scintillation light signal S1 together with the charge signal S2 allowed to lower the energy threshold already by one order of magnitude down to 0.4 keV and the cross section limit by many orders of magnitude. Cryogenic bolometers can have even lower energy thresholds (e.g. CRESST-III [48]), but they suffer from much smaller detector masses. In addition, alternative technologies such as the charge-coupled-device (CCD) experiments SENSEI [67] and DAMIC [68] with 0.1 kg to 1 kg (1K) target mass, respectively, a low-threshold Generation-2 (G2+) SuperCDMS detector [69] or a superconducting Aluminum cube [70] are currently being explored [65]. The liquid xenon experiment LBECA also aims at a significant background reduction for single or few electron signals [66]. Note that the current limits, e.g. from the first shallow underground run of SENSEI, are still eight orders of magnitude weaker than the projected sensitivity [67]. The projections are therefore shown in Fig. 9 as dashed lines.

7 Conclusion

Motivated by the observations of DM, fundamental scalars and non-zero neutrino masses in Nature, we have studied in this paper right-handed neutrinos with MeV to GeV mass, that can explain the DM and generate the active neutrino masses at one loop through their couplings to the SM neutrinos via a dark scalar doublet, mixing with a scalar singlet. When the mass of the lightest neutral scalar is also as light as MeV (*i.e.* a so-called SLIM), this scotogenic model, as had been observed previously, can in addition solve the cosmological missing satellite, cusp-core and the too-big-to fail problems.

We first scanned the full parameter space with right-handed neutrino DM in the MeV to GeV mass range to identify viable models that reproduce the observed SM neutrino mass differences and lead to the correct observed relic density. We found that these models automatically have DM masses above a few MeV in excellent agreement with bounds from big-bang nucleosynthesis. We also observed that they implied sizeable couplings to not only the neutral, but also the charged SM leptons between a few times 10^{-4} and a few times 10^{-1} .

We then turned to lepton flavour violation, which had previously not been analysed, but which occurs naturally in this type of models due to the coupling of the dark sector to both the charged and neutral SM leptons. Specifically, we calculated the expected branching ratio of the process $\mu \rightarrow e\gamma$, which is usually the most sensitive one. This process turned out to

be highly constraining, with the current MEG results already eliminating a substantial part of the lepton coupling parameter space. Since the latter is constrained from below from the requirement of non-zero active neutrino masses, the planned MEG upgrade should almost completely verify or exclude this model. The current limits on the processes $\mu \rightarrow 3e$ and muon to electron conversion in Titanium proved to be less constraining, but the next generation of experiments should be of similar sensitivity.

Since no nuclear recoil signal was expected for this leptophilic DM, we then investigated instead the possibility of an electron signal, which had generally been suggested as a possible way to detect sub-GeV DM. We found that, despite the sizeable coupling of the right-handed neutrino DM to charged leptons, the electron recoil cross section did not exceed a few times 10^{-46} cm², when all low-energy, collider, cosmological and neutrino mass and mixing constraints were imposed. This result could be traced to the fact that the charged scalar mediator was restricted by LEP searches to be heavier than 98.5 GeV and suppressed the cross section with the fourth power of the mass. Lepton flavour violation constraints limited the electron recoil cross section further down to at most 10^{-52} cm². We furthermore performed a detailed study of the sensitivity of XENON and other direct detection experiments, in particular to DM induced electron recoil for a 1 ton-year exposure collected with realistic backgrounds and energy thresholds, and compared it to previous theoretical estimates without backgrounds or threshold limitations. Here, we found that cross sections of about 10^{-36} cm² rather than a few times 10^{-41} cm² and DM masses of a few 100 MeV rather than a few tens of MeV were required. Furthermore, we included the recent published S2-only analysis result from XENON1T that features a lower electron energy threshold of 0.4 keV and a simplified, but realistic background model. The cross sections of about 10^{-39} cm² for DM masses a few tens of MeV demonstrated several orders of magnitude of improvement in the XENON sensitivity, approaching the optimistic theoretical estimates. This makes it imperative to increase the exposure in the future at a threshold below the keV level, *e.g.* by exploiting further only the ionisation (S2) signal. There, XENONnT will rival the sensitivities of upcoming or planned dedicated experiments exploring the MeV mass range such as SENSEI, DAMIC-1K, SuperCDMS-G2+ or superconducting Aluminum cubes. We cautioned again that theoretical projections may be overly optimistic, as they were in the case of XENON, since *e.g.* the proven sensitivity from the first underground run of SENSEI is still eight orders of magnitude below the projection.

We close with two remarks on possible generalisations of this model and future directions of research. Indeed, some of our findings do not depend on the details of the model. In particular, our results should apply more generally to MeV to GeV scale neutrino DM and depend neither on the details of the symmetry stabilising the DM nor on the presence of an equally light scalar, as the main feature was the coupling of MeV neutrino DM to SM leptons via the scalar doublet and the LEP limit on the mass of its charged component. In contrast, promoting the $U(1)$ symmetry stabilising the DM to a local symmetry and then studying the phenomenology of its spontaneous breaking at colliders and in cosmology would represent an interesting future direction of research [71].

Acknowledgements

We thank J. Alvey for useful discussions. This work has been supported by the BMBF under contract 05H18PMCC1 and the DFG through the Research Training Group 2149 “Strong and weak interactions – from hadrons to dark matter”.

References

- [1] M. Klasen, M. Pohl and G. Sigl, *Prog. Part. Nucl. Phys.* **85** (2015) 1.
- [2] N. Aghanim *et al.* [Planck Collaboration], arXiv:1807.06209 [astro-ph.CO].
- [3] G. Jungman, M. Kamionkowski and K. Griest, *Phys. Rept.* **267** (1996) 195.
- [4] B. Herrmann, M. Klasen *et al.*, *Phys. Rev. D* **76** (2007) 117704; *Phys. Rev. D* **79** (2009) 061701; *Phys. Rev. D* **80** (2009) 085025; *Phys. Rev. D* **87** (2013) 054031; *Phys. Rev. D* **89** (2014) 114012; *Phys. Rev. D* **91** (2015) 034028; *Phys. Rev. D* **91** (2015) 034012; *Phys. Rev. D* **93** (2016) 114023; *Phys. Rev. D* **99** (2019) 095015.
- [5] F. Boudjema *et al.*, *Phys. Lett. B* **660** (2008) 550; *Phys. Rev. D* **81** (2010) 015005; *Phys. Rev. D* **84** (2011) 116001; *Phys. Rev. D* **89** (2014) 115020.
- [6] M. Beneke, C. Hellmann *et al.*, *JHEP* **1503** (2015) 162; *JHEP* **1505** (2015) 115; *JHEP* **1603** (2016) 119
- [7] M. Klasen, K. Kovarik and P. Steppeler, *Phys. Rev. D* **94** (2016) 095002.
- [8] B. Fuks, M. Klasen *et al.*, *Phys. Lett. B* **688** (2010) 208; *Nucl. Phys. B* **842** (2011) 51; *Nucl. Phys. B* **849** (2011) 64; *JHEP* **1210** (2012) 081; *Eur. Phys. J. C* **73** (2013) 2480; *JHEP* **1607** (2016) 053; *Phys. Rev. D* **98** (2018) 055014.
- [9] E. Aprile *et al.* [XENON Collaboration], *Phys. Rev. Lett.* **121** (2018) 111302.
- [10] V. Dutta, S.L. Williams, F. Alonso, talks at EPS HEP 2019, Ghent, Belgium.
- [11] G. Aad *et al.* [ATLAS Collaboration], *Phys. Lett. B* **716** (2012) 1.
- [12] S. Chatrchyan *et al.* [CMS Collaboration], *Phys. Lett. B* **716** (2012) 30.
- [13] L. Lopez Honorez, E. Nezri, J. F. Oliver and M. H. G. Tytgat, *JCAP* **0702** (2007) 028.
- [14] M. Klasen, C. E. Yaguna and J. D. Ruiz-Alvarez, *Phys. Rev. D* **87** (2013) 075025.
- [15] A. Goudelis, B. Herrmann and O. Stal, *JHEP* **1309** (2013) 106.
- [16] M. Tanabashi *et al.* [Particle Data Group], *Phys. Rev. D* **98** (2018) 030001.
- [17] E. Ma, *Phys. Rev. D* **73** (2006) 077301.
- [18] D. Restrepo, O. Zapata and C. E. Yaguna, *JHEP* **1311** (2013) 011
- [19] M. Klasen *et al.*, *JCAP* **1304** (2013) 044; *Eur. Phys. J. C* **78** (2018) 88; *JHEP* **1810** (2018) 055; *JHEP* **1905** (2019) 015 and references cited therein.
- [20] V. Springel *et al.*, *Nature* **435** (2005) 629.
- [21] M. Drewes *et al.*, *JCAP* **1701** (2017) 025.
- [22] C. Boehm, Y. Farzan, T. Hambye, S. Palomares-Ruiz and S. Pascoli, *Phys. Rev. D* **77** (2008) 043516.
- [23] Y. Farzan, *Phys. Rev. D* **80** (2009) 073009; *Int. J. Mod. Phys. A* **26** (2011) 2461.

- [24] C. Boehm, D. Hooper, J. Silk, M. Casse and J. Paul, Phys. Rev. Lett. **92** (2004) 101301.
- [25] A. Arhrib, C. Boehm, E. Ma and T. C. Yuan, JCAP **1604** (2016) 049
- [26] J. Kubo, E. Ma and D. Suematsu, Phys. Lett. B **642** (2006) 18.
- [27] J. Kopp, V. Niro, T. Schwetz and J. Zupan, Phys. Rev. D **80** (2009) 083502; D. Schmidt, T. Schwetz and T. Toma, Phys. Rev. D **85** (2012) 073009; P. H. Gu and X. G. He, Phys. Lett. B **778** (2018) 292.
- [28] R. Essig, J. Mardon and T. Volansky, Phys. Rev. D **85** (2012) 076007; R. Essig, A. Manalaysay, J. Mardon, P. Sorensen and T. Volansky, Phys. Rev. Lett. **109** (2012) 021301; R. Essig, M. Fernandez-Serra, J. Mardon, A. Soto, T. Volansky and T. T. Yu, JHEP **1605** 046 (2016); R. Essig, T. Volansky and T. T. Yu, Phys. Rev. D **96** (2017) 043017.
- [29] S. K. Lee, M. Lisanti, S. Mishra-Sharma and B. R. Safdi, Phys. Rev. D **92** (2015) 083517.
- [30] M. Aaboud *et al.* [ATLAS Collaboration], Phys. Rev. Lett. **122** (2019) 231801.
- [31] A. M. Sirunyan *et al.* [CMS Collaboration], Phys. Lett. B **793** (2019) 520.
- [32] G. Abbiendi *et al.* [OPAL Collaboration], Phys. Lett. B **572** (2003) 8.
- [33] A. M. Sirunyan *et al.* [CMS Collaboration], Eur. Phys. J. C **79** (2019) 421.
- [34] C. Boehm, P. Fayet and R. Schaeffer, Phys. Lett. B **518** (2001) 8.
- [35] C. Boehm and R. Schaeffer, Astron. Astrophys. **438** (2005) 419.
- [36] J. A. Casas and A. Ibarra, Nucl. Phys. B **618** (2001) 171.
- [37] S. May, M.Sc. thesis, University of Münster, 2018.
- [38] F. Staub, Comput. Phys. Commun. **185** (2014) 1773.
- [39] W. Porod and F. Staub, Comput. Phys. Commun. **183** (2012) 2458.
- [40] D. Barducci, G. Belanger, J. Bernon, F. Boudjema, J. Da Silva, S. Kraml, U. Laa and A. Pukhov, Comput. Phys. Commun. **222** (2018) 327.
- [41] A. M. Baldini *et al.* [MEG Collaboration], Eur. Phys. J. C **76** (2016) 434.
- [42] F. Renga [MEG Collaboration], Hyperfine Interact. **239** (2018) 58.
- [43] U. Bellgardt *et al.* [SINDRUM Collaboration], Nucl. Phys. B **299** (1988) 1.
- [44] C. Dohmen *et al.* [SINDRUM II Collaboration], Phys. Lett. B **317** (1993) 631.
- [45] A. Blondel *et al.*, arXiv:1301.6113 [physics.ins-det].
- [46] A. Sato, PoS NUFACT **08** (2008) 105.
- [47] E. Aprile *et al.* [XENON Collaboration], Phys. Rev. D **94** (2016) 092001. Erratum: [Phys. Rev. D **95** (2017) 059901].
- [48] A. H. Abdelhameed *et al.* [CRESST Collaboration], arXiv:1904.00498 [astro-ph.CO].
- [49] J. I. Read, J. Phys. G **41** (2014) 063101.
- [50] C. F. Bunge, J. A. Barrientos and A. V. Bunge, Atom. Data Nucl. Data Tabl. **53** (1993) 113.
- [51] M. C. Smith *et al.*, Mon. Not. Roy. Astron. Soc. **379** 755 (2007).
- [52] P. F. Depta, M. Hufnagel, K. Schmidt-Hoberg and S. Wild, JCAP **1904** (2019) 029.
- [53] L. Baudis, H. Dujmovic, C. Geis, A. James, A. Kish, A. Manalaysay, T. Marrodan Undagoitia and M. Schumann, Phys. Rev. D **87** (2013) 115015.

- [54] E. Aprile *et al.* [XENON Collaboration], JCAP **1604** 027 (2016).
- [55] E. Aprile *et al.* [XENON Collaboration], Eur. Phys. J. C **77** 275 (2017).
- [56] E. Aprile *et al.* [XENON100 Collaboration], Phys. Rev. D **90** 062009 (2014). Erratum: [Phys. Rev. D **95** 029904 (2017)].
- [57] M. Szydagis *et al.*, JINST **6**, P10002 (2011).
- [58] E. Aprile *et al.* [XENON Collaboration], arXiv:1902.11297 [physics.ins-det].
- [59] G. J. Feldman and R. D. Cousins, Phys. Rev. D **57** (1998) 3873.
- [60] E. Aprile *et al.* [XENON100 Collaboration], Science **349** (2015) 851.
- [61] E. Aprile *et al.* [XENON100 Collaboration], J. Phys. G **41** (2014) 035201.
- [62] J. Angle *et al.* [XENON10 Collaboration], Phys. Rev. Lett. **107** (2011) 051301. Erratum: [Phys. Rev. Lett. **110** (2013) 249901].
- [63] E. Aprile *et al.* [XENON Collaboration], arXiv:1907.11485 [hep-ex].
- [64] P. Agnes *et al.* [DarkSide Collaboration], Phys. Rev. Lett. **121** (2018) 111303.
- [65] M. Battaglieri *et al.*, arXiv:1707.04591 [hep-ph].
- [66] K. Ni, talk given at TAUP 2019, Toyoma, Japan, <http://www-kam2.icrr.u-tokyo.ac.jp/indico/event/3/session/45/contribution/390/material/slides/0.pdf>.
- [67] O. Abramoff *et al.* [SENSEI Collaboration], Phys. Rev. Lett. **122** (2019) 161801.
- [68] A. Aguilar-Arevalo *et al.* [DAMIC Collaboration], Phys. Rev. Lett. **118** (2017) 141803.
- [69] R. Agnese *et al.* [SuperCDMS Collaboration], Phys. Rev. Lett. **116** (2016) 071301.
- [70] Y. Hochberg, M. Pyle, Y. Zhao and K. M. Zurek, JHEP **1608** (2016) 057.
- [71] M. Klasen, F. Lyonnet and F. S. Queiroz, Eur. Phys. J. C **77** (2017) 348; D. A. Camargo, M. D. Campos, T. B. de Melo and F. S. Queiroz, Phys. Lett. B **795** (2019) 319; D. A. Camargo, M. Klasen and S. Zeinstra, arXiv:1903.02572 [hep-ph].